Dalton Transactions

Accepted Manuscript

ROYAL SOCIETY OF CHEMISTRY

www.rsc.org/dalton

A wide range color-tunable tri-chromatic $Ca_9Sc(PO_4)_7$: Eu^{2+}, Tb^{3+}, Mn^{2+} w-LED phosphor was obtained based on the efficient Eu^{2+} to Tb^{3+} and Eu^{2+} to Mn^{2+} energy transfer processes.

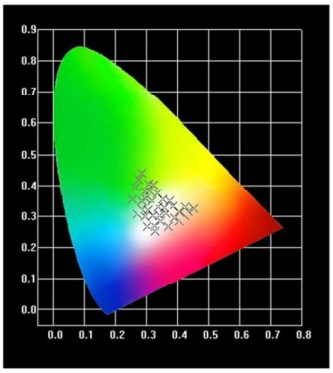

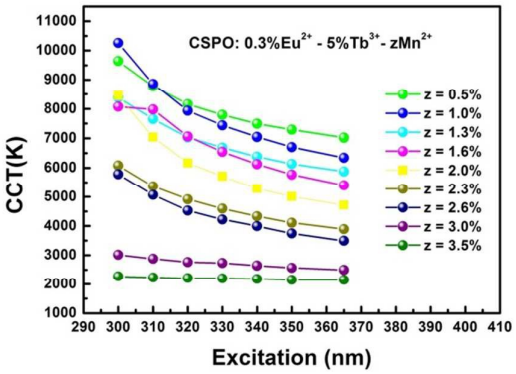

Journal Name

RSCPublishing

ARTICLE

Tri-chromatic white-light emission from a single-phase $Ca_9Sc(PO_4)_7$: Eu^{2+}, Tb^{3+}, Mn^{2+} phosphor for LED applications

Cite this: DOI: 10.1039/x0xx00000x

Lihong Jiang,[a] Ran Pang,[a] Da Li,[a] Wenzhi Sun,[a, b] Yonglei Jia,[a, b] Haifeng Li,[a, b] Jipeng Fu,[a, b] Chengyu Li,*[a] Su Zhang,*[a]

Received 00th January 2012,
Accepted 00th January 2012

DOI: 10.1039/x0xx00000x

www.rsc.org/

A series of single-phase $Ca_9Sc(PO_4)_7$: Eu^{2+}, Tb^{3+}, Mn^{2+} phosphors for UV excitations were synthesized by high-temperature solid-state reaction. Energy transfer from Eu^{2+}→Tb^{3+} and Eu^{2+}→Mn^{2+} in $Ca_9Sc(PO_4)_7$ sample is a feasible route to realize color-tunable emission because $Ca_9Sc(PO_4)_7$ single-doped Eu^{2+}/Tb^{3+}/Mn^{2+} emit blue, green and red lights, respectively. Most of the white light region in CIE chromaticity diagram has been realized in $Ca_9Sc(PO_4)_7$: Eu^{2+}, Tb^{3+}, Mn^{2+} phosphors. Warm white lights including the points of (0.337, 0.331), (0.353, 0.355) and (0.358, 0.327) close to day light (0.33, 0.33) with CCT of 5285 K, 4719 K and 4333 K are obtained, respectively.

1. Introduction

White light emitting diodes (w-LEDs) are considered to be the next-generation light source and will replace conventional incandescent or fluorescence lamps due to their advantages of being mercury-free, energy saving, high luminescence efficiency, long life, environmentally friendly features, etc.[1-3] At present, w-LEDs can be fabricated by using a blue InGaN LED chip in combination with a yellow phosphor of Ce^{3+}-doped yttrium aluminum garnet (YAG: Ce). However, this phosphor exhibits a poor color rendering index (CRI) and a highly correlated color temperature (CCT) due to the lack of a red light emission which serious limit the white color quality.[4-6] To solve this problem, green and red phosphors in combination with a blue LED or red, green and blue phosphors combined with a UV LED have been suggested as alternatives.[7-9] However, different degradation rates of chip and phosphors result in chromatic aberration and poor color stability for longer working times. Therefore, it is necessary to develop a single-phase tri-chromatic (red/green/blue) emission phosphor that can be efficiently excited by UV or near-UV light for the fabrication of w-LED.

One of the approaches for generating white light from single-phase phosphors is by doping multi rare-earth ions, as co-doping sensitizers and activators, into the same host. It is well known that there have been several reports about the photoluminescence (PL) properties of Ce^{3+}, Eu^{2+}, Tb^{3+} and Mn^{2+} and the energy transfer mechanisms of sensitizer/activator pairs, such as Eu^{2+}/Mn^{2+}, Eu^{2+}/Tb^{3+}, Eu^{2+}/Mn^{2+}/Tb^{3+}, Ce^{3+}/Mn^{2+}, Ce^{3+}/Tb^{3+} and Ce^{3+}/Mn^{2+}/Tb^{3+} have been investigated in many hosts.[10-22]

As far as we know, the crystal structures and luminescence properties of $Ca_9Sc(PO_4)_7$ (CSPO) have not yet been reported. In this article, we report a novel single-phase tri-chromatic white-light-emitting phosphor, $Ca_9Sc(PO_4)_7$: Eu^{2+}, Tb^{3+}, Mn^{2+}, in which the energy transfer mechanism between blue-emitting Eu^{2+}, green-emitting Tb^{3+} and red-emitting Mn^{2+} in the host and the luminescence properties are firstly investigated. A wide range color-tunable tri-chromatic emission was obtained by adjusting not only the Eu^{2+}, Tb^{3+}, and Mn^{2+} contents, but also the excitation wavelength because the excitation spectra of Eu^{2+}/Tb^{3+}/Mn^{2+} in $Ca_9Sc(PO_4)_7$ host are different. In addition, most of the white light region in CIE chromaticity diagram has been realized in CSPO: Eu^{2+}, Tb^{3+}, Mn^{2+} phosphors. Warm white lights including the points of (0.337, 0.331), (0.353, 0.355) and (0.358, 0.327) close to day light (0.33, 0.33) with CCT of 5285 K, 4719 K and 4333 K are obtained, respectively.

2. Experimental

2.1 Materials and Synthesis

The $Ca_9Sc(PO_4)_7$ host and a series of rare-earth doped $Ca_9Sc(PO_4)_7$ phosphors were prepared by a high-temperature solid-state reaction technique. The raw materials were $CaCO_3$ (A. R.), Sc_2O_3(A. R.), $NH_4H_2PO_4$(A. R.), Eu_2O_3(99.99%), Tb_4O_7 (99.99%) and $MnCO_3$ (A. R.). Stoichiometric amounts of the raw materials were mixed and thoroughly ground in an agate mortar. The powder mixtures were sintered at 500 ℃ for 10h in an alumina crucible. After cooling down to room

temperature, the samples were re-ground and finally sintered at 1200℃ for 10 h in a reducing atmosphere of H_2/N_2 (5%/95%).

2.2 Materials Characterization

The powder X-ray diffraction (XRD) data were obtained by a Bruker D8 focus diffractometer with graphite-monochromatized Cu Ka radiation (k = 0.15405 nm) operating at 40 kV and 40 mA, at a scanning rate of 0.8° min^{-1} in the 2θ range from 10° to 120 °. The photoluminescence (PL) and photoluminescence excitation (PLE) spectra were measured with a Hitachi F-7000 spectrophotometer equipped with the excitation source of a 150W xenon lamp. The luminescence decay curve was obtained from a Lecroy Wave Runner 6100 digital oscilloscope (1 GHz) using a tunable laser (pulse width = 4 ns, gate = 50 ns) as the excitation source (Continuum Sunlite OPO).

3. Results and discussion

3.1 Crystal Structure

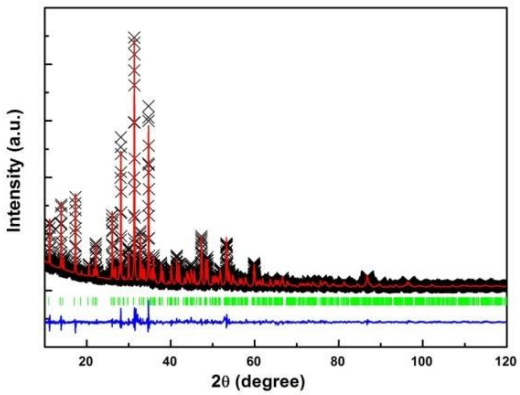

Figure 1 Observed (black crosses), calculated (red solid line), and difference (blue solid line) XRD profiles for the Rietveld refinement of $Ca_9Sc(PO_4)_7$.

The phase purity of the as-prepared powder samples were first examined by XRD. Figure 1 shows the observed (black crosses), calculated (red solid line), and difference (blue solid line) XRD profiles for the Rietveld refinement of CSPO host sintered at 1200℃ for 10h in H_2/N_2 (5%/95%) conducted using the GSAS program. The Rietveld refinement results indicate that no other phase or impurity can be detected in CSPO host structure. The CSPO crystallizes as a hexagonal structure with space group *R3c*. For CSPO, the lattice parameters were determined to be *a* = 10.4165 Å, *b* = 10.4165 Å, *c* = 37.3783 Å, V = 3512.34 $Å^3$ and the refinement finally converged to R_p (%) = 8.12, R_{wp} (%) = 5.48, and χ^2 = 5.16, which was shown in Table 1.

$Ca_9Sc(PO_4)_7$ is known to be based on the structure of *β*-$Ca_3(PO_4)_2$-type compounds (space group *R3c*) which have six metal sites, *M*1-*M*6, and three P sites, P1-P3. *M*1, *M*2, *M*3, P2 and P3 occupy general positions (18*b*) while *M*4, *M*5, *M*6 and P1 are located at (6*a*) sites on the threefold rotation axis.[23] $Ca_9Sc(PO_4)_7$ is isostructural to $Ca_9Fe(PO_4)_7$ and an investigation of the structure of $Ca_9Fe(PO_4)_7$ has shown that Ca^{2+} ions occupy the *M*1-*M*3 sites of the *β*-$Ca_3(PO_4)_2$ -type structure, Fe^{3+} ions are located in the *M*5 sites, while the *M*4 and *M*6 sites are vacant.[24] The simulation of the crystal structure of $Ca_9Sc(PO_4)_7$ is shown in Figure 2. The crystal structure of $Ca_9Sc(PO_4)_7$ indicates that each cation has different coordination environments, for example, Ca1, Ca2 and Ca3 atoms located at 18*b* sites are eight-coordinated by oxygen atoms, with an average distance of 2.5548 Å, 2.5090 Å and 2.4658 Å respectively, while Sc^{3+} located at 6*a* sites are six-coordinated by oxygen atoms, with an average distance of 2.2192 Å, each ScO_6 octahedron is linked to two different PO_4^{3-} groups. The PO_4^{3-} tetrahedral in $Ca_9Sc(PO_4)_7$ is isolated like PO_4^{3-} groups in other whitlockite-like phosphates.[25] According to the similar effective ionic radius and valence of cations,[10,26-29] we suggest that Eu^{2+} (r = 1.25 Å for CN = 8) and Mn^{2+} (r = 0.96 Å for CN = 8) prefer to occupy Ca^{2+} (r = 1.12 Å for CN = 8) sites while Tb^{3+} (r = 0.923 Å for CN = 6) replaces Sc^{3+} (r = 0.745 Å for CN = 6) more easily.

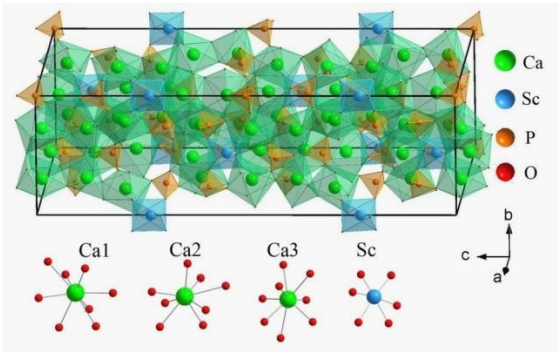

Figure 2 Crystal structure of $Ca_9Sc(PO_4)_7$.

Table 1 Rietveld Refinement and Crystal Data of $Ca_9Sc(PO_4)_7$ host.

$Ca_9Sc(PO_4)_7$			
Crystal symmetry:	hexagonal		
Space group:	*R3c*		
Z	6		
Cell parameters:	*a* = 10.4165(2) Å	*b* = 10.4165(4) Å	*c* = 37.3783(8) Å
	α = 90°	*β* = 90°	*γ* = 120°
Cell volume:	3512.34(26) $Å^3$		
	χ^2 = 5.16	R_p (%) = 8.12	R_{wp} (%) = 5.48

3.2 Photoluminescence properties

Figure 3 shows the PL and PLE spectra of CSPO: $0.003Eu^{2+}$. It is observed that under excitation at 292 nm, the PL spectrum of CSPO: $0.003Eu^{2+}$ exhibits a broad band emission from 360 to 650 nm, which corresponds to the $4f^65d^1 \rightarrow 4f^7$ transition of the Eu^{2+} ions. The emission spectrum can be decomposed into three Gaussian profiles with peaks located at 414 nm, 444 nm and 510 nm. These peaks indicate that there are three emission centers in CSPO: $0.003Eu^{2+}$ lattice, which could be identified as the different coordination environments of Ca^{2+} ions being occupied by Eu^{2+} ions. As shown in Figure 2, three different Ca^{2+} sites exist in CSPO: $0.003Eu^{2+}$ crystal structure, Ca1, Ca2

and Ca3 ions located at 18*b* sites are eight-coordinated by oxygen atoms, with an average distance of 2.5548 Å, 2.5090 Å and 2.4658 Å respectively. The splitting of the 5d excited state of Eu^{2+} strongly depends on the strength of the crystal field, which is inversely proportional to R^5 (*R*: chemical bond length between a cation with d orbital electrons and the coordinating anion).[30] Thus, the Eu^{2+} ions substituting the Ca^{2+} sites with a shorter Ca-O bond distance will experience stronger crystal field strength corresponding to a longer wavelength emission. Hence, we infer that the band at 414 nm (assigned to Eu (1)), is occupying Ca1 sites with a weakest crystal field, and the other bands at 444 nm (assigned to Eu (2)), 510 nm (assigned to Eu (3)), are occupying Ca2 and Ca3, respectively.

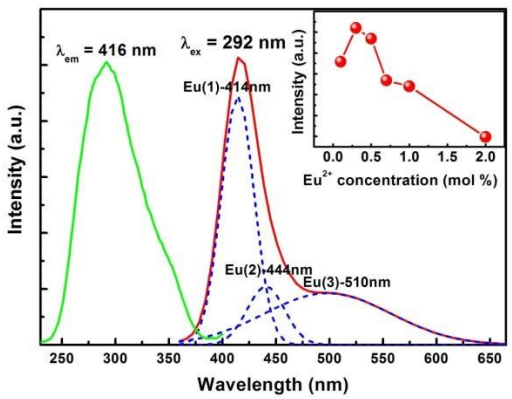

Figure 3 PL and PLE spectra of CSPO: 0.003Eu^{2+} sample and the deconvoluted emission spectra of three Gaussian bands. The inset shows the PL intensity as a function of Eu^{2+} content for CSPO: xEu^{2+} under excitation at 292 nm.

The inset of Figure 3 shows the PL intensity of CSPO with different doping concentration of Eu^{2+} ions. It can be observed that the emission intensity of Eu^{2+} ions first increases with increasing doping concentration, reaching a maximum at x = 0.3, and then decreases sharply with increasing concentration due to the concentration quenching effect. The critical distance *Rc* between Eu^{2+} ions can be estimated using the relation given by Blasse.[31]

$$Rc = 2\left[\frac{3V}{4\pi XcN}\right]^{1/3} \quad (1)$$

Where *V* is the volume of the unit cell, *N* is the number of host cations in the unit cell, and *Xc* is the critical concentration of Eu^{2+} ions. For the $Ca_9Sc(PO_4)_7$ host, *N* = 54 and *V* = 3512.34 $Å^3$, *Xc* is 0.003. Therefore, the critical distance (*Rc*) is calculated to be about 34.6 Å.

It is well known that the ground state of the Tb^{3+} ion with a $4f^8$ electron configuration is on the $^7F_6$ level, and its $4f^75d^1$ excitation levels have high-spin (HS) ^9D_J and the low-spin (LS) ^7D_J states. As a result, the excitation spectrum of Tb^{3+} ion generally exhibits two groups of f - d transitions.[32] Figure 4 (a) shows the excitation spectrum of CSPO: 5% Tb^{3+} sample. It shows a strong broad band located at 233 nm with a shoulder at 264 nm which may due to a spin-allowed $4f^8 \rightarrow 4f^75d^1$ ($\triangle S = 0$) transition and a spin-forbidden $4f^8 \rightarrow 4f^75d^1$ ($\triangle S = 1$) transition, respectively.[26] Moreover, there are several transitions from 278 to 500 nm, which are due to the intra-$4f^8$ transitions from the $^7F_6$ to the $^5F_{5,4}$, $^5H_{7-4}$, $^5D_{1,0}$, $^5L_{10-7}$, $^5G_{6-2}$, $^5D_{2-4}$ levels. Figure 4 (b) shows the emission spectra of CSPO doped with different Tb^{3+} ion concentrations. It can be seen that the Tb^{3+} emission peaks at 383, 412, 436, 457 and 472 nm attribute to $^5D_3 \rightarrow {}^7F_{2-6}$ transitions; and peaks at 489, 543, 588 and 623 nm attribute to $^5D_4 \rightarrow {}^7F_{3-6}$ transitions. It is clear that the emission spectra show different ratios between the $^5D_3$ and $^5D_4$ emissions at lower and higher Tb^{3+} concentrations. The emission spectrum for low Tb^{3+} concentrations consists of the transitions from both the $^5D_3$ and $^5D_4$ levels. With the increase of Tb^{3+} concentration, the emissions from the $^5D_3$ to the ^7F_J levels are quenched gradually by the cross-relaxation process between neighboring Tb^{3+} ions.[33, 34] For the Tb^{3+} ion, the energy gap between the $^5D_3$ and $^5D_4$ levels is close to that between the $^7F_6$ and $^7F_0$ levels. Hence, if the Tb^{3+} concentrations is high enough , the high energy level emission can be easily quenched in favor of the lower energy level emission, i.e. Tb^{3+} ($^5D_3$) + Tb^{3+} ($^7F_6$) → Tb^{3+} ($^5D_4$) + Tb^{3+} ($^7F_0$), accompanied by enhancement of the emission from the $^5D_4$ level.[35]

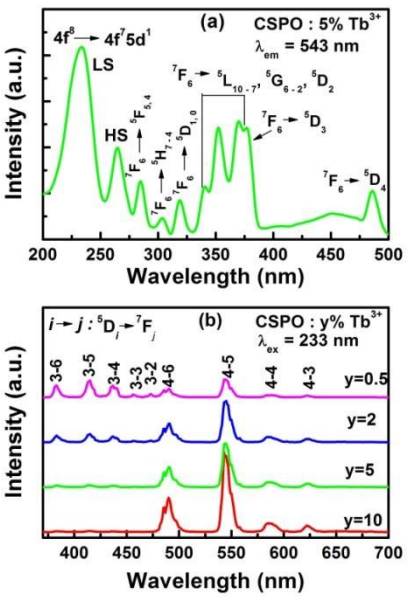

Figure 4 Photoluminescence excitation spectrum of CSPO: 5% Tb^{3+} sample (a) and photoluminescence emission spectra of CSPO: y% Tb^{3+} with different Tb^{3+} ion concentrations (b).

Figure 5 (a) shows the PL spectrum of CSPO: 0.003 Eu^{2+} and the PLE spectrum of CSPO: 0.05 Tb^{3+}. It is clearly observed that there is an overlap between the emission spectrum of Eu^{2+} and the excitation spectrum of Tb^{3+}, which indicates that the energy transfer may occur from Eu^{2+} to Tb^{3+} in CSPO: Eu^{2+}, Tb^{3+} samples. The excitation spectrum monitoring with the Tb^{3+} $^5D_4$ - $^7F_5$ transition (543 nm) of CSPO: Eu^{2+}, Tb^{3+} sample, as shown in Figure 5 (b), consists of not only the Eu^{2+} excitation bands but also the Tb^{3+} excitation bands. The first band attributed to absorptions of Tb^{3+} $4f^8 \rightarrow$ $4f^75d$ transitions and the latter (250 - 450 nm) is due to the

transitions of Eu^{2+} $4f^7 \rightarrow 4f^6 5d$. The presence of the Eu^{2+} absorption band suggests that the energy transfer from Eu^{2+} to Tb^{3+} can be expected to take place in CSPO host. The PL spectrum of CSPO: Eu^{2+}, Tb^{3+} excited at 292 nm exhibits a broad blue emission band and several line emission, attributed to the $5d \rightarrow 4f$ transition of Eu^{2+} and $^5D_4 \rightarrow {}^7F_J$ (J = 3, 4, 5, 6) transitions of Tb^{3+}, respectively.

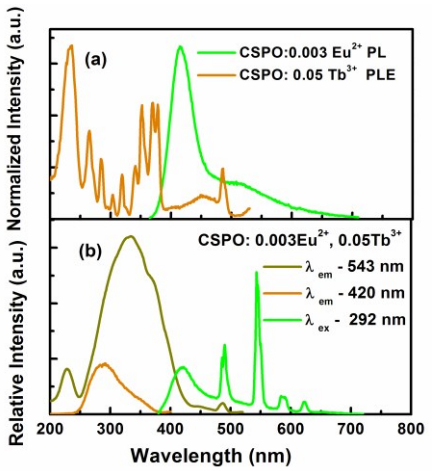

Figure 5 (a) The PL spectrum of CSPO: 0.003 Eu^{2+} and the PLE spectrum of CSPO: 0.05 Tb^{3+}; (b) the PL (excited at 292 nm) and PLE (monitored at 543nm and 420 nm) spectra of Eu^{2+}, Tb^{3+} co-doped CSPO.

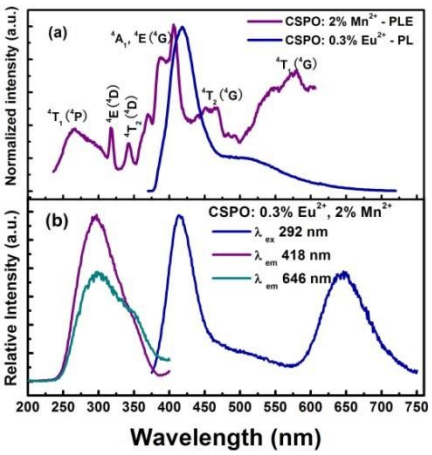

Figure 6 (a) The PL spectrum of CSPO: 0.003 Eu^{2+} and the PLE spectrum of CSPO: 0.02 Mn^{2+}; (b) the PL (excited at 292 nm) and PLE (monitored at 646nm and 418 nm) spectra of Eu^{2+}, Mn^{2+} co-doped CSPO.

The PL spectrum of CSPO: 0.003 Eu^{2+} and the PLE spectrum of CSPO: 0.02 Mn^{2+} are shown in Figure 6 (a). The PLE spectrum of Mn^{2+} consists of several broad bands and peaks in the range of 230 - 600 nm due to the transitions of the Mn^{2+} ion from ground state $^6A_1$ (^6S) to the crystal field components of the excited $^4T_1$ (^4P), ^4E (^4D), $^4T_2$ (^4D), $^4A_1$, ^4E (^4G), $^4T_2$ (^4G) and $^4T_1$ (^4G) levels.[36] As seen in Figure 6 (a), we observe a significant spectral overlap between the Eu^{2+} PL and Mn^{2+} PLE spectra, indicating that the emission of spectrum of Eu^{2+} ions matches with the excitation spectrum of Mn^{2+} ions. Hence, an effective energy transfer from Eu^{2+} to Mn^{2+} ion was expected. Figure 6 (b) shows the PL and PLE spectral of CSPO: 0.003Eu^{2+}, 0.02Mn^{2+}. The broad band emissions around 418 (blue band) and 646 nm (red band) excited by 292 nm are due to the 5d→4f transition of the Eu^{2+} ion and the spin-forbidden $^4T_1$ (^4G) → $^6A_1$ (^6S) transition of the Mn^{2+} ion, respectively. Moreover, another evidence for energy transfer in CSPO: 0.003Eu^{2+}, 0.02Mn^{2+} is that the PLE spectral monitoring the emission of Mn^{2+} and the emission of Eu^{2+} are similar.

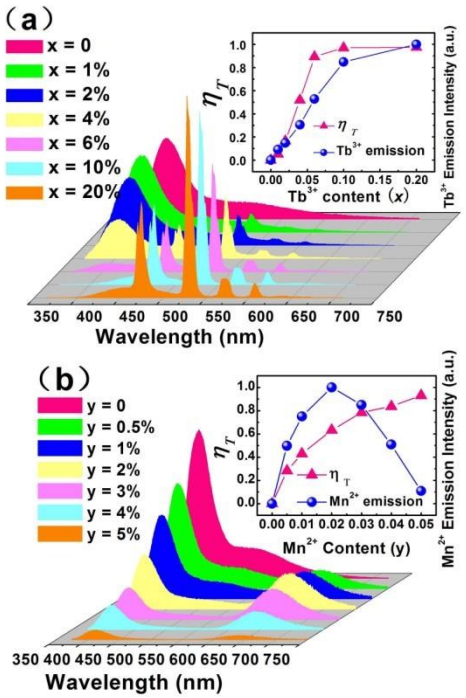

Figure 7 The PL spectra of (a) CSPO: 0.003 Eu^{2+}, x Tb^{3+} (λ_{ex} = 292 nm) and (b) CSPO: 0.003 Eu^{2+}, y Mn^{2+} (λ_{ex} = 292 nm). The insets show the dependence of Tb^{3+}/Mn^{2+} PL intensity and energy transfer efficiency on changing Tb^{3+} and Mn^{2+} contents.

Figure 7(a) shows the emission spectra of the CSPO: 0.003 Eu^{2+}, x Tb^{3+} with different Tb^{3+} doping concentrations from 0 to 20% excited by 292 nm. Although the concentration of Eu^{2+} was fixed at 0.3%, the emission intensity for Eu^{2+} decreased with increasing Tb^{3+} concentration, whereas the emission intensity for Tb^{3+} increases with increases of its concentration. The above results indicate that there exists efficient energy transfer from Eu^{2+} to Tb^{3+}. Moreover, different intensity of blue emission from Eu^{2+} or green emission from Tb^{3+} can be obtained by adjusting appropriately the concentration of the sensitizer Eu^{2+} and the activator Tb^{3+}. In addition, we found that Tb^{3+} ions do not show typical concentration quenching behaviour at high concentration of 20% Tb^{3+}. The reason for this phenomenon in CSPO: 0.003 Eu^{2+}, xTb^{3+} phosphor may be that Tb^{3+} ions occupy Sc^{3+} sites in the CSPO host while the ions distance of Sc^{3+} was obviously longer than that of Ca^{2+} as shown in Fig. 2. Hence, a lower concentration quenching effect can be expected from this phosphor. The quenching concentration may be very high. The similar phenomena were also observed in other materials, e.g.,

$Sr_{3.5}Y_{6.5}O_2(PO_4)_{1.5}(SiO_4)_{4.5}$: Ce^{3+}, Tb^{3+}, Mn^{2+}, $KCaGd(PO_4)_2$: Eu^{2+}, Tb^{3+}, Mn^{2+}, $Sr_3In(PO_4)_3$: Ce^{3+}, Tb^{3+}, Mn^{2+}, $Ba_3LaNa(PO_4)_3F$: Eu^{2+}, Tb^{3+}.[1,26,37,38] The quenching concentration of Tb^{3+} was 40% in Jiao's reports about $Ba_3LaNa(PO_4)_3F$: Eu^{2+}, Tb^{3+}.[38]

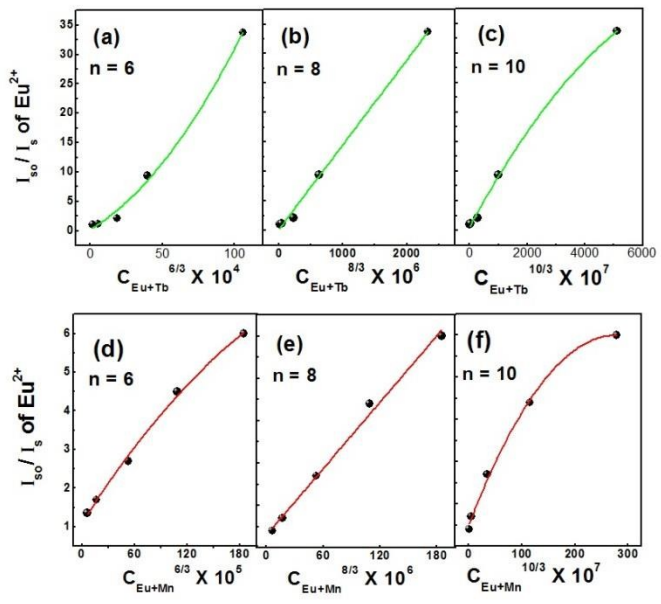

Figure 8 Dependence of I_{so}/I_s of Eu^{2+} on (a) $C_{Eu+Tb}^{6/3}$ (b) $C_{Eu+Tb}^{8/3}$ (c) $C_{Eu+Tb}^{10/3}$ (d) $C_{Eu+Mn}^{6/3}$ (e) $C_{Eu+Mn}^{8/3}$ (f) $C_{Eu+Mn}^{10/3}$.

The energy transfer efficiency η_T from a sensitizer (Eu^{2+}) to an activator (Tb^{3+}) in CSPO: 0.003 Eu^{2+}, x Tb^{3+} phosphors can be expressed through the following equation: [39, 40]

$$\eta_T = 1 - \frac{I_S}{I_{S0}} \qquad (2)$$

Where η_T is the energy transfer efficiency and I_S and I_{S0} are the luminescence intensity of the sensitizer Eu^{2+} ions in the presence and absence of the activator Tb^{3+} ions, respectively. As a consequence, the η_T values from Eu^{2+} to Tb^{3+} were calculated to be 0, 5.25%, 16.5%, 51.88%, 89.36%, 97.04% and 97.55% for CSPO: 0.003 Eu^{2+}, x Tb^{3+} phosphors and plotted as a function of x (x = 0, 0.01, 0.02, 0.04, 0.06, 0.1, 0.2), as shown in inset of Figure 7 (a). In general, there are two main aspects which are responsible for the resonant ET mechanism: one is exchange interactions and the other is multipolar interactions.[41, 42] We know that if ET results from the exchange interactions, the critical distance between the sensitizer and activator should be shorter than 4Å.[42] The critical distance *Rc* for ET from the Eu^{2+} to Tb^{3+} ions can also be calculated using eqn (1). Here, *X* is the total concentration of Eu^{2+} and Tb^{3+} ions, and the critical concentration (*Xc*) is that at which the luminescence intensity of the sensitizer (Eu^{2+}) is half that in the sample in the absence of the activator (Tb^{3+}), that is to say, *Xc* occurs when $\eta_T = 0.5$. For the $Ca_9Sc(PO_4)_7$: Eu^{2+}, Tb^{3+} system, the critical concentration *Xc* is 4.1%. Hence, the critical distance (*Rc*) of ET was calculated to be about 14.47 Å. It is observed that the radiative emission from Eu^{2+} prevails when $R_{Eu\text{-}Tb} > Rc$ and ET from Eu^{2+} to Tb^{3+} dominates when $R_{Eu\text{-}Tb} < Rc$. This value is much longer than 4 Å, indicating little possibility of ET *via* the exchange interaction mechanism. Hence, the electric multipolar interaction can take place for ET between the Eu^{2+} and Tb^{3+} ions. According to Dexter's ET expressions of multipolar interaction and Reisfeld's approximation, the following relation can be given: [31, 41, 43]

$$\frac{\eta_0}{\eta} \propto C_{Eu+Tb}^{n/3} \qquad (3)$$

Where η_0 and η is the luminescence quantum efficiency of Eu^{2+} ions without and with the activator (Tb^{3+}) present; the values of η_0/η can be approximately calculated by the ratio of related luminescence intensities (I_0/I); C_{Eu+Tb} is the total dopant concentration of Eu^{2+} and Tb^{3+}; and n = 6, 8, and 10, are dipole-dipole, dipole-quadrupole, and quadrupole-quadrupole interactions, respectively. The $I_0/I - C_{Ce+Tb}^{n/3}$ plots are further illustrated in Figure 8 (a)–(c), and the relationships are observed when n = 6, 8 and 10. Only when n = 8 does it show a linear relation. This clearly indicates that the ET from the Eu^{2+} to Tb^{3+} ions is the dipole-quadrupole mechanism. Therefore, the electric dipole-quadrupole interaction predominates in the ET process from Eu^{2+} to Tb^{3+} ions in the CSPO host. Considering the dipole-quadrupole interaction, the critical distance from the sensitizer to activator can also be calculated by the spectral overlap method, as expressed as follows: [44]

$$R_c^8 = 3.024 \times 10^{12} \lambda s^2 f_q \int \frac{F_S(E) F_A(E)}{E^4} dE \qquad (4)$$

Where f_q is the oscillator strength of the Tb^{3+} electric quadrupole transition, λs (in Å) is the wavelength position of the sensitizer's emission, E is the energy involved in the transfer (in eV), and $\int F_S(E) F_A(E) dE/E$ represents the spectral overlap between the normalized shapes of the Eu^{2+} emission $F_S(E)$ and the Tb^{3+} excitation $F_A(E)$, and in our case it is calculated to be about 0.0882 eV^{-4}. It is a pity that the oscillator strength of the Tb^{3+} quadrupole transition (f_q) has not been obtained up to now. However, it was suggested by Verstegen *et al.* that the ratio f_q/f_d is about 10^{-3} to10^{-2}, where $f_d = 10^{-6}$ is the oscillator strength of the Tb^{3+} electric dipole transition.[45] Using eqn (4), the critical distance R_C for the dipole-quadrupole interaction method is 16.14–21.53 Å. We assumed the ratio $f_q/f_d = 10^{-3}$, the critical distance R_C was estimated to be 16.14Å, which agrees approximately with that obtained by using the concentration-quenching method (14.47Å).

Figure 7(b) depicts the PL of the CSPO: 0.003 Eu^{2+}, yMn^{2+} samples with varying Mn^{2+} concentrations from 0 to 5% under excitation at 292 nm. With increasing the Mn^{2+} concentration, it is found that the emission intensity of Eu^{2+} ions decreases from y = 0 to 0.05, while the emission intensity of Mn^{2+} ions increases initially and reaches a maximum at y = 0.02, beyond which it decreases due to the Mn^{2+}-Mn^{2+} internal concentration quenching. Hence, the η_T values from Eu^{2+} to Mn^{2+} were calculated to be 0, 28.33%, 42.96%, 63.22%, 78.39%, 83.63% and 93.09% for CSPO: 0.003 Eu^{2+}, y Mn^{2+}

phosphors and plotted as a function of y (y = 0, 0.005, 0.01, 0.02, 0.03, 0.04, 0.05), as shown in inset of Figure 7 (b). The critical distance (R_C) of ET between the Eu^{2+} and Mn^{2+} ions calculated by the quenching concentration method (eqn(1)) and the spectral overlap method (eqn(4)) are 19.4Å and 14.4Å, respectively. According to eqn(4), when n = 8 the I_0/I – $C_{Ce+Mn}^{n/3}$ plots show a linear relation as shown in Figure 8 (d) – (f). This powerfully indicates that the ET from Eu^{2+} to Mn^{2+} ions also has the dipole-quadrupole mechanism.

The inset of Figure 7 (a) and Figure 7 (b) exhibit the increasing trend of η_T value of Eu^{2+}→Tb^{3+}/Mn^{2+} while the increasing rate decreases because the fixed Eu^{2+} concentration restricts the energy transfer from Eu^{2+}.

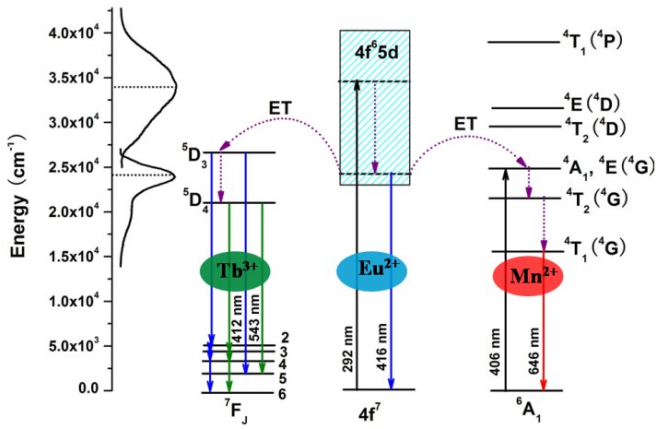

Figure 9 The schematic level diagram for energy transfer process in the $Ca_9Sc(PO_4)_7$ host. The PLE (λ_{em} = 416 nm) and PL (λ_{ex} = 292 nm) spectra of CSPO: 0.003 Eu^{2+} phosphor are also shown as a reference.

Figure 9 illustrates the energy level schemes of Eu^{2+}/Tb^{3+}/Mn^{2+} and the possible energy transfer models for Eu^{2+}→Tb^{3+} and Eu^{2+}→Mn^{2+} in the $Ca_9Sc(PO_4)_7$ host. The PLE (λ_{em} = 416 nm) and PL (λ_{ex} = 292 nm) spectra of CSPO: 0.003Eu^{2+} is also shown in Figure 9 as a reference. As shown in Figure 9, the 5d band of Eu^{2+} overlaps partially the excited-state energy levels of Mn^{2+} ($^4A_1$, ^4E (^4G)) and Tb^{3+} ($^5D_3$), indicating the energy transfer between Eu^{2+}→Mn^{2+} and Eu^{2+}→Tb^{3+} may occur *via* nonradiative transitions. When the Eu^{2+} ion is irradiated by UV light, electron is pumped to higher component of 5d level and nonradiatively relaxes to the lowest 5d crystal field splitting state, and then it return to the ground state ($4f^7$) with a 416 nm emission. As the similar values of the energy levels, an energy transfer is expected to take place from the excited 5d state of Eu^{2+} to $^4A_1$, ^4E (^4G) level of Mn^{2+} and ($^5D_3$) level of Tb^{3+} in the $Ca_9Sc(PO_4)_7$ host. Mn^{2+} ion receives the energy transferred from excited Eu^{2+}, the electrons in the Mn^{2+} ion from the ground state are excited into $^4A_1$, ^4E (^4G) energy levels. Then, the excited free electron relaxes to the excited state $^4T_1$ (^4G) through $^4T_2$ (^4G) intermediate energy level in a nonradiative process, followed by a radiative transition from excited state of $^4T_1$ (^4G) to the ground state of $^6A_1$ (^6S), with a typical emission of Mn^{2+} located at 646 nm. At the same time, the luminescence intensity of Eu^{2+} decreases. With the increasing of Mn^{2+} concentration, the energy transfer from Eu^{2+} to Mn^{2+} increases and the intensity of Eu^{2+} decreases gradually, as shown in Figure 7 (b). The energy transfer of Eu^{2+}→Tb^{3+} is similar to Eu^{2+}→Mn^{2+}. The excited Eu^{2+} ions transfer energy to $^5D_3$ level of Tb^{3+} ions; subsequently, the $^5D_3$ level gives its characteristic transitions or continues to transfer the energy to the $^5D_4$ level *via* cross relaxation. Then a set of characteristic transitions of $^5D_4$ →$^7F_{3\text{-}6}$, located at 489, 543, 588 and 623 nm, are exhibited.

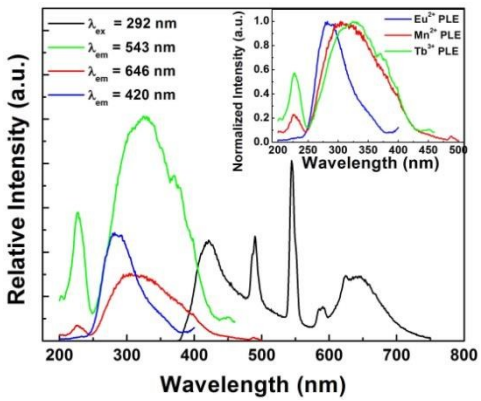

Figure 10 PL and PLE spectra of CSPO: 0.3% Eu^{2+}, 5% Tb^{3+}, 1.6 % Mn^{2+}. The inset shows the excitation spectra of Eu^{2+}/Tb^{3+}/Mn^{2+} of CSPO: 0.3% Eu^{2+}, 5% Tb^{3+}, 1.6 % Mn^{2+} phosphor.

A white light emission can be obtained through mixing the tricolor (RGB) lights at a suitable ratio. Based on previous studies, energy transfer from Eu^{2+}→Tb^{3+} and Eu^{2+}→Mn^{2+} in CSPO sample is a feasible route to realize color-tunable emission because CSPO single-doped Eu^{2+}/Tb^{3+}/Mn^{2+} emit blue, green and red lights, respectively. Figure 10 shows PL and PLE spectra of CSPO: 0.3% Eu^{2+}, 5% Tb^{3+}, 1.6 % Mn^{2+}. The PL spectrum of CSPO: 0.3% Eu^{2+}, 5% Tb^{3+}, 1.6% Mn^{2+} sample is composed of blue emission of Eu^{2+}, green emission of Tb^{3+}, and red emission of Mn^{2+}. Therefore, color-tunable phosphors can be obtained by adjusting the content of Tb^{3+} and Mn^{2+}. Moreover, as shown in the inset of Figure 10, the main excitation peaks of Eu^{2+}/Tb^{3+}/Mn^{2+} in CSPO: 0.3% Eu^{2+}, 5% Tb^{3+}, 1.6 % Mn^{2+} phosphor locate at 292 nm, 315 nm, and 331 nm, respectively, which attribute to the transitions of Eu^{2+} $4f^7$-$4f^6$5d. Obviously, in comparison with Eu^{2+}, there is some red shift for the main peak of PLE spectra of Tb^{3+} and Mn^{2+}. Hence, the emission intensity of Eu^{2+}/Tb^{3+}/Mn^{2+} is various when excited at different wavelength.

Figure 11 (a) shows the PL spectra of CSPO: 0.3% Eu^{2+}, 5% Tb^{3+}, z % Mn^{2+} (z = 0.1%, 0.5%, 1.6%, 2.3%) excited at 300 nm. With increasing Mn^{2+} concentration, the PL intensity of the Mn^{2+} emission is found to increase, and that of Eu^{2+} and Tb^{3+} are observed to decrease. Figure 11 (b) shows PL spectra of CSPO: 0.3% Eu^{2+}, 5% Tb^{3+}, 1.6% Mn^{2+} excited at different wavelength (λ_{ex} = 300 nm, 320 nm, 340 nm, 365 nm). Obviously, with increasing excitation wavelength, the variety trend of PL intensity of Eu^{2+}/Tb^{3+}/Mn^{2+} is different. Therefore, color-tunable phosphors can also be obtained by adjusting the excitation wavelength.

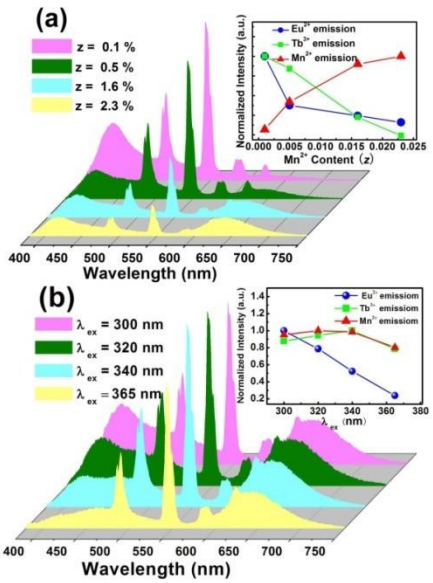

Figure 11 (a) PL spectra of CSPO: 0.3% Eu^{2+}, 5% Tb^{3+}, z % Mn^{2+} (z = 0.1%, 0.5%, 1.6%, 2.3%) excited at 300 nm; (b) PL spectra of CSPO: 0.3% Eu^{2+}, 5% Tb^{3+}, 1.6% Mn^{2+} excited at different wavelength (λ_{ex} = 300 nm, 320 nm, 340 nm, 365 nm).

In order to further validate the $Eu^{2+} \rightarrow Tb^{3+}$ and $Eu^{2+} \rightarrow Mn^{2+}$ energy transfer process in the $Ca_9Sc(PO_4)_7$ host lattice, the PL decay curves of Eu^{2+} in CSPO: Eu^{2+}, xTb^{3+}, yMn^{2+} phosphors, together with the calculated lifetimes are shown in Figure 12. The luminescent decay times can be fitted well with a second-order exponential decay curve by the following equation:

$$I(t) = A_1 \, exp(-t/\tau_1) + A_2 \, exp(-t/\tau_2) \qquad (3)$$

Where $I(t)$ is the luminescence intensity at time t; A_1 and A_2 are constants; τ_1 and τ_2 are rapid and slow lifetimes for the exponential components, respectively. Using these parameters, the average decay time (τ) can be determined by the formula as follows:

$$\tau = (A_1 {\tau_1}^2 + A_2 {\tau_2}^2) \, / (A_1 \tau_1 + A_2 \tau_2) \qquad (4)$$

Based on the above equation (4), the average decay times (τ) are calculated to be 0.7380, 0.6962, 0.6682, 0.4644, 0.3133 and 0.2060 μs for CSPO: Eu^{2+}, xTb^{3+}, yMn^{2+} with x = 0, y = 0; x = 2%, y = 0; x = 5%, y = 0; x = 5%, y = 0.5%; x = 5%, y = 1.6%; x = 5%, y = 2.3%, respectively. It can be seen that the decay lifetime of the Eu^{2+} ions decreases monotonically with an increase in Tb^{3+} and Mn^{2+} doping concentrations, which strongly demonstrates the energy transfer from Eu^{2+} to Tb^{3+} and Mn^{2+} ions.

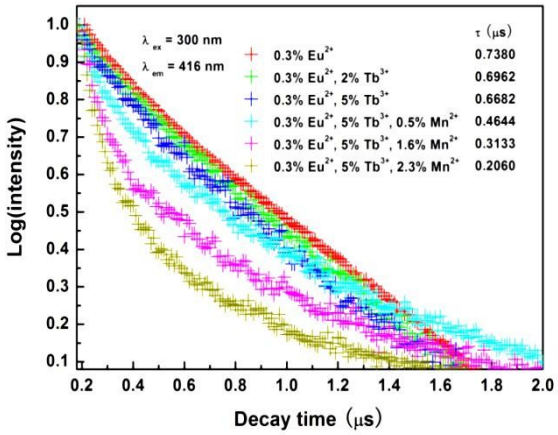

Figure 12 PL decay curves of Eu^{2+} in CSPO: 0.003Eu^{2+}, xTb^{3+}, yMn^{2+} phosphors displayed on a logarithmic intensity scale.

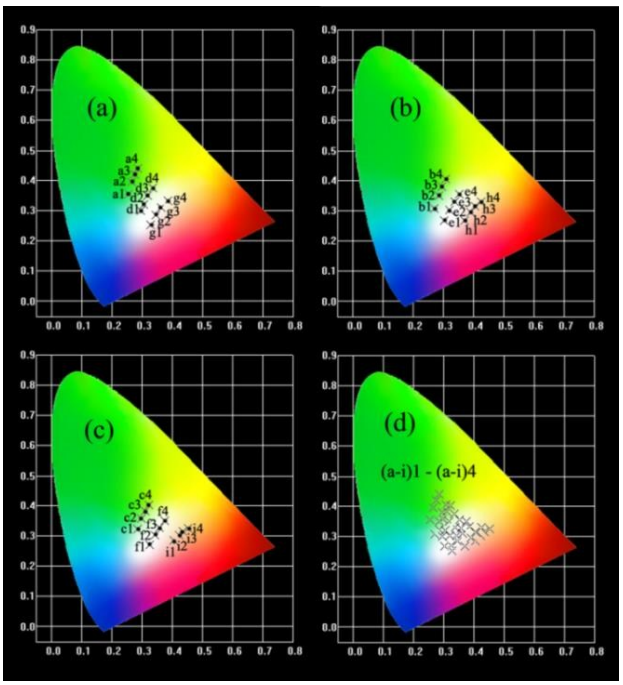

Figure 13 CIE chromaticity diagram of CSPO: 0.003Eu^{2+}, 0.05Tb^{3+}, yMn^{2+} phosphors at different excitation (a) (a1-a4: y = 0.005; d1-d4: y = 0.016; g1-g4: y = 0.026); (b) (b1-b4: y = 0.01; e1-e4: y = 0.02; h1-h4: y = 0.03); (c) (c1-c4: y = 0.013; f1-f4: y = 0.023; i1-i4: y = 0.035); (d) the combination of (a), (b) and (c). λ_{ex} = 300, 320, 340 and 365 nm.

A series of warm white light phosphors can be obtained via adjusting not only the concentrations of Eu^{2+}/Tb^{3+}/Mn^{2+}, but also the excited wavelength. The Commission International de L'Eclairage (CIE) chromaticity diagram of CSPO: Eu^{2+}, 0.05Tb^{3+}, yMn^{2+} phosphors at different excitation wavelength are measured, and the results are shown in Figure 13 and Table 2. The results show that most of the white light region in CIE chromaticity diagram has been realized in CSPO: Eu^{2+}, 0.05Tb^{3+}, yMn^{2+} phosphors with adjusting the Mn^{2+} content and the excitation wavelength. As we all know, a warm white light with correlated color temperature (CCT) below 5000K is popular in solid state lighting. Figure 14 shows the CCT of

CSPO: Eu^{2+}, $0.05Tb^{3+}$, yMn^{2+} phosphors excited at different wavelength. Obviously, The CCT basically exhibits a decrease trend with increasing the content of Mn^{2+} (red emission) and the excitation wavelength, respectively. As shown in Figure 13, the as-synthesized CSPO: Eu^{2+}, $0.05Tb^{3+}$, yMn^{2+} phosphors include the points of e3 (0.337, 0.331), e4 (0.353, 0.355) and f3 (0.358, 0.327) close to day liht (0.33, 0.33) with CCT of 5285 K, 4719 K and 4333 K, respectively.

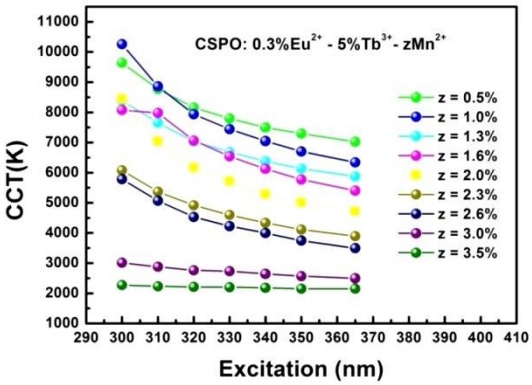

Figure 14 CCT of CSPO: Eu^{2+}, $0.05Tb^{3+}$, zMn^{2+} (z = 0.5%, 1.0%, 1.3%, 1.6%, 2.0%, 2.3%, 2.6%, 3.0%, 3.5%) phosphors excited at different wavelength.

Table 2 The CIE chromaticity diagram of CSPO: Eu2+, 0.05Tb3+, yMn2+ phosphors at different excitation wavelength

No. of the point in the CIE diagram	Sample compositions	Excitation (nm)	QE (%)	CIE (*x*, *y*)	CCT (*K*)
a 1	CSPO:0.003Eu^{2+}, 0.05Tb^{3+}, 0.005Mn^{2+}	300	54.9	(0.254, 0.354)	9644
a 2	CSPO:0.003Eu^{2+}, 0.05Tb^{3+}, 0.005Mn^{2+}	320	37.9	(0.266, 0.395)	8158
a 3	CSPO:0.003Eu^{2+}, 0.05Tb^{3+}, 0.005Mn^{2+}	340	34.1	(0.275, 0.420)	7494
a 4	CSPO:0.003Eu^{2+}, 0.05Tb^{3+}, 0.005Mn^{2+}	365	32.5	(0.284, 0.441)	7023
b 1	CSPO:0.003Eu^{2+}, 0.05Tb^{3+}, 0.010Mn^{2+}	300	52.0	(0.269, 0.307)	10260
b 2	CSPO:0.003Eu^{2+}, 0.05Tb^{3+}, 0.010Mn^{2+}	320	38.3	(0.284, 0.349)	7939
b 3	CSPO:0.003Eu^{2+}, 0.05Tb^{3+}, 0.010Mn^{2+}	340	39.3	(0.294, 0.379)	7046
b 4	CSPO:0.003Eu^{2+}, 0.05Tb^{3+}, 0.010Mn^{2+}	365	28.7	(0.308, 0.406)	6340
c 1	CSPO:0.003Eu^{2+}, 0.05Tb^{3+}, 0.013Mn^{2+}	300	52.3	(0.285, 0.322)	8386
c 2	CSPO:0.003Eu^{2+}, 0.05Tb^{3+}, 0.013Mn^{2+}	320	37.2	(0.298, 0.358)	7032
c 3	CSPO:0.003Eu^{2+}, 0.05Tb^{3+}, 0.013Mn^{2+}	340	33.0	(0.310, 0.383)	6378
c 4	CSPO:0.003Eu^{2+}, 0.05Tb^{3+}, 0.013Mn^{2+}	365	30.6	(0.322, 0.403)	5874
d 1	CSPO:0.003Eu^{2+}, 0.05Tb^{3+}, 0.016Mn^{2+}	300	40.6	(0.296, 0.300)	8078
d 2	CSPO:0.003Eu^{2+}, 0.05Tb^{3+}, 0.016Mn^{2+}	320	30.4	(0.305, 0.320)	7061
d 3	CSPO:0.003Eu^{2+}, 0.05Tb^{3+}, 0.016Mn^{2+}	340	26.8	(0.318, 0.349)	6124
d 4	CSPO:0.003Eu^{2+}, 0.05Tb^{3+}, 0.016Mn^{2+}	365	26.9	(0.336, 0.376)	5400
e 1	CSPO:0.003Eu^{2+}, 0.05Tb^{3+}, 0.020Mn^{2+}	300	52.2	(0.302, 0.267)	8452
e 2	CSPO:0.003Eu^{2+}, 0.05Tb^{3+}, 0.020Mn^{2+}	320	33.9	(0.321, 0.302)	6165
e 3	CSPO:0.003Eu^{2+}, 0.05Tb^{3+}, 0.020Mn^{2+}	340	27.2	(0.337, 0.331)	5285
e 4	CSPO:0.003Eu^{2+}, 0.05Tb^{3+}, 0.020Mn^{2+}	365	22.2	(0.353, 0.355)	4719
f 1	CSPO:0.003Eu^{2+}, 0.05Tb^{3+}, 0.023Mn^{2+}	300	39.8	(0.324, 0.270)	6077
f 2	CSPO:0.003Eu^{2+}, 0.05Tb^{3+}, 0.023Mn^{2+}	320	30.8	(0.342, 0.302)	4916
f 3	CSPO:0.003Eu^{2+}, 0.05Tb^{3+}, 0.023Mn^{2+}	340	25.5	(0.358, 0.327)	4333
f 4	CSPO:0.003Eu^{2+}, 0.05Tb^{3+}, 0.023Mn^{2+}	365	23.0	(0.376, 0.349)	3893
g 1	CSPO:0.003Eu^{2+}, 0.05Tb^{3+}, 0.026Mn^{2+}	300	41.6	(0.328, 0.253)	5781
g 2	CSPO:0.003Eu^{2+}, 0.05Tb^{3+}, 0.026Mn^{2+}	320	37.1	(0.346, 0.284)	4528
g 3	CSPO:0.003Eu^{2+}, 0.05Tb^{3+}, 0.026Mn^{2+}	340	31.8	(0.362, 0.310)	3997
g 4	CSPO:0.003Eu^{2+}, 0.05Tb^{3+}, 0.026Mn^{2+}	365	24.3	(0.384, 0.333)	3496
h 1	CSPO:0.003Eu^{2+}, 0.05Tb^{3+}, 0.030Mn^{2+}	300	39.6	(0.369, 0.268)	3009
h 2	CSPO:0.003Eu^{2+}, 0.05Tb^{3+}, 0.030Mn^{2+}	320	31.6	(0.390, 0.296)	2759
h 3	CSPO:0.003Eu^{2+}, 0.05Tb^{3+}, 0.030Mn^{2+}	340	36.7	(0.406, 0.315)	2642
h 4	CSPO:0.003Eu^{2+}, 0.05Tb^{3+}, 0.030Mn^{2+}	365	25.0	(0.424, 0.331)	2497
i 1	CSPO:0.003Eu^{2+}, 0.05Tb^{3+}, 0.035Mn^{2+}	300	31.8	(0.404, 0.284)	2273
i 2	CSPO:0.003Eu^{2+}, 0.05Tb^{3+}, 0.035Mn^{2+}	320	26.4	(0.422, 0.302)	2212
i 3	CSPO:0.003Eu^{2+}, 0.05Tb^{3+}, 0.035Mn^{2+}	340	26.8	(0.436, 0.314)	2183
i 4	CSPO:0.003Eu^{2+}, 0.05Tb^{3+}, 0.035Mn^{2+}	365	22.0	(0.453, 0.326)	2151

4. Conclusions

In summary, we have synthesized a novel single-phase tri-chromatic white-light-emitting phosphor $Ca_9Sc(PO_4)_7$: Eu^{2+}, Tb^{3+}, Mn^{2+}. A wide range color-tunable tri-chromatic emission was obtained by adjusting not only the Eu^{2+}, Tb^{3+}, and Mn^{2+} contents, but also the excitation wavelength, which is due to the efficient $Eu^{2+}\rightarrow Tb^{3+}$ and $Eu^{2+}\rightarrow Mn^{2+}$ energy transfer processes. Most of the white light region in CIE chromaticity diagram has been realized in CSPO: $0.003Eu^{2+}$, $0.05Tb^{3+}$, yMn^{2+} phosphors with adjusting the Mn^{2+} content and the excitation wavelength. Warm white lights including the points of (0.337, 0.331), (0.353, 0.355) and (0.358, 0.327) close to day light (0.33, 0.33) with CCT of 5285 K, 4719 K and 4333 K are obtained, respectively.

5. Acknowledgements

The authors are grateful to the financial aid from Hong Kong, Macao and Taiwan Science and Technology Cooperation Special Project of Ministry of Science and Technology of People's Republic of China (Grant no. 2014DFT10310), Program of Science and Technology Development Plan of Jilin Province of China (Grant No 20140201007GX), National Natural Science Foundation of China (Grant Nos. 51102229, 51402288, 21401184).

[a] State Key Laboratory of Application of Rare Earth Resources, Changchun Institute of Applied Chemistry, Chinese Academy of Sciences, Changchun 130022, China
[b] University of Chinese Academy of Sciences, Beijing 100049, PR China

References

1. W. R. Liu, C. H. Huang, C. W. Yeh, Y. C. Chiu, Y. T. Yeh and R. S. Liu, RSC Advances, 2013, 3, 9023.
2. X. Zhang and M. Gong, Dalton Transactions, 2014, 43, 2465.
3. W. Lu, Y. Jia, W. Lv, Q. Zhao and H. You, RSC Advances, 2013, 3, 20619.
4. Z. Hao, J. Zhang, X. Zhang, X. Sun, Y. Luo, S. Lu and X. J. Wang, Applied Physics Letters, 2007, 90, 261113.
5. J. S. Kim, P. E. Jeon, Y. H. Park, J. C. Choi, H. L. Park, G. C. Kim and T. W. Kim, Applied Physics Letters, 2004, 85, 3696.
6. W. J. Yang and T. M. Chen, Applied Physics Letters, 2007, 90, 171908.
7. G. Y. Lee, J. Y. Han, W. B. Im, S. H. Cheong and D. Y. Jeon, Inorganic Chemistry, 2012, 51, 10688.
8. J. Y. Han, W. B. Im, G. Y. Lee and D. Y. Jeon, Journal of Materials Chemistry, 2012, 22, 8793.
9. C. H. Huang, D. Y. Wang, Y. C. Chiu, Y. T. Yeh and T. M. Chen, RSC Advances, 2012, 2, 9130.
10. X. Chen, P. Dai, X. Zhang, C. Li, S. Lu, X. Wang, Y. Jia and Y. Liu, Inorganic Chemistry, 2014, 53, 3441.
11. H. Liu, Y. Luo, Z. Mao, L. Liao and Z. Xia, Journal of Materials Chemistry C, 2014, 2, 1619.
12. C. H. Huang, P. J. Wu, J. F. Lee and T. M. Chen, Journal of Materials Chemistry, 2011, 21, 10489.
13. J. Sun, Z. Lian, G. Shen and D. Shen, RSC Advances, 2013, 3, 18395.
14. N. Guo, Y. Zheng, Y. Jia, H. Qiao and H. You, New Journal of Chemistry, 2012, 36, 168.
15. J. Yu, Z. Hao, X. Zhang, Y. Luo and J. Zhang, Chemical Communications, 2011, 47, 12376.
16. K. Li, D. Geng, M. Shang, Y. Zhang, H. Lian and J. Lin, The Journal of Physical Chemistry C, 2014, 118, 11026.
17. K. Li, M. Shang, Y, Zhang, J. Fan, H. Lian, J. Lin, The Journal of Physical Chemistry C, 2015, 3, 7096.
18. M. Shang, C. Li, J. Lin, Chemical Society Reviews, 2014, 43, 1372.
19. K. Li, Y. Zhang, X. Li, M. Shang, H. Lian, J. Lin, Dalton Transactions, 2015, 44, 4683.
20. W. Ding, J. Wang, Z. Liu, M. Zhang, Q. Su, J. Tang, Journal of The Electrochemical Society, 2008, 155, J122.
21. X. Zhang, L. Huang, F. Pan, M. Wu, J. Wang, Y. Chen, Q. Su, Applied Materials & Interfaces, 2014, 6, 2709.
22. X. Zhang, J. Wang, L. Huang, F. pan, Y. Chen, B. Li, M. Peng, M. Wu, Applied Materials & Interfaces, 2015, 7, 10044.
23. A. A. Belik, F. Izumi, T. Ikeda, M. Okui, A. P. Malakho, V. A. Morozov and B. I. Lazoryak, Journal of Solid State Chemistry, 2002, 168, 237.
24. V. A. Morozov, A. A. Belik, S. Y. Stefanovich, V. V. Grebenev, O. I. Lebedev, G. Van Tendeloo and B. I. Lazoryak, Journal of Solid State Chemistry, 2002, 165, 278.
25. B. I. Lazoryak, V. A. Morozov, A. A. Belik, S. S. Khasanov and V. S. Shekhtman, Journal of Solid State Chemistry, 1996, 122, 15.
26. D. Geng, G. Li, M. Shang, D. Yang, Y. Zhang, Z. Cheng and J. Lin, Journal of Materials Chemistry, 2012, 22, 14262.
27. C. Huang, Y. Chiu, Y. Yeh, T. Chan, T. Chen, Applied Materials & Interfaces, 2012, 4, 6661.
28. K. Li, J. Fan, X. Mi, Y. Zhang, H. Lian, M. Shang, J. Lin, Inorganic Chemistry, 2014, 53, 12141.
29. Y. Chen, Y. Li, J. Wang, M. Wu, C. Wang, The Journal of Physical Chemistry C, 2014, 118, 12494.
30. X. Piao, T. Horikawa, H. Hanzawa and K. i. Machida, Applied Physics Letters, 2006, 88, 161908.
31. G. Blasse, Philips Res. Rep., 1969, 24, 131.
32. N. Guo, Y. Song, H. You, G. Jia, M. Yang, K. Liu, Y. Zheng, Y. Huang and H. Zhang, European Journal of Inorganic Chemistry, 2010, 2010, 4636.
33. B. C. G. G. Blasse, Springer-Verlag, Berlin and Heidelberg, 1994, ch. 4.
34. K. S. Sohn, Y. Y. Choi, H. D. Park and Y. G. Choi, Journal of The Electrochemical Society, 2000, 147, 2375.
35. X. Liu and J. Lin, Journal of Materials Chemistry, 2008, 18, 221.
36. H. Tada, Q. Jin, A. Iwaszuk and M. Nolan, The Journal of Physical Chemistry C, 2014, 118, 12077.
37. H. Liu, Y. Luo, Z. Mao, L. Liao, Z. Xia, The Journal of Physical Chemistry C, 2014, 2, 1619.
38. M. Jiao, N. Guo, W. Lu, Y. Jia, L. Lv, Q. Zhao, B. Shao, H. You, Inorganic Chemistry, 2013, 52, 10340.
39. K. H. Kwon, W. B. Im, H. S. Jang, H. S. Yoo and D. Y. Jeon, Inorganic Chemistry, 2009, 48, 11525.
40. P. I. Paulose, G. Jose, V. Thomas, N. V. Unnikrishnan and M. K. R. Warrier, Journal of Physics and Chemistry of Solids, 2003, 64, 841.
41. R. Reisfeld, E. Greenberg, R. Velapoldi, B. Barnett, The Journal of Chemical Physics, 1972, 56, 1698.
42. B. M. Antipeuko, I. M. Bataev, V. L. Ermolaev, E. I. Lyubimov, T. A. Privalova, optics and spectroscopy, 1970, 29, 177.
43. D. L. Dexter, J. A. Schulman, The Journal of Chemical Physics, 1954, 22, 1063.
44. S. Nakamura, G. Fasol, The Blue Laser Diode, Springer, Berlin, 1996.
45. J. M. P. J. Verstegen, J. L. Sommerdijk, J.G. Verriet, Journal of luminescence, 1973, 6, 425.